ORIGINAL PAPER



Experimental study of quartz inclusions in garnet at pressures up to 3.0 GPa: evaluating validity of the quartz-in-garnet inclusion elastic thermobarometer

Jay B. Thomas 10 · Frank S. Spear 2

Received: 22 November 2017 / Accepted: 17 April 2018 © Springer-Verlag GmbH Germany, part of Springer Nature 2018

Abstract

Garnet crystals with quartz inclusions were hydrothermally crystallized from oxide starting materials in piston-cylinder apparatuses at pressures from 0.5 to 3 GPa and temperatures ranging from 700 to 800 °C to study how entrapment conditions affect remnant pressures of quartz inclusions used for quartz-in-garnet (QuiG) elastic thermobarometry. Systematic changes of the 128, 206 and 464 cm⁻¹ Raman band frequencies of quartz were used to determine pressures of quartz inclusions in garnet using Raman spectroscopy calibrations that describe the P-T dependencies of Raman band shifts for quartz under hydrostatic pressure. Within analytical uncertainties, inclusion pressures calculated for each of the three Raman band frequencies are equivalent, which suggests that non-hydrostatic stress effects caused by elastic anisotropy in quartz are smaller than measurement errors. The experimental quartz inclusions have pressures ranging from -0.351 to 1.247 GPa that span the range of values observed for quartz inclusions in garnets from natural rocks. Quartz inclusion pressures were used to model P-T conditions at which the inclusions could have been trapped. The accuracy of QuiG thermobarometry was evaluated by considering the differences between pressures measured during experiments and pressures calculated using published equation of state parameters for quartz and garnet. Our experimental results demonstrate that Raman measurements performed at room temperature can be used without corrections to estimate garnet crystallization pressures. Calculated entrapment pressures for quartz inclusions in garnet are less than ~ 10\% different from pressures measured during the experiments. Because the method is simple to apply with reasonable accuracy, we expect widespread usage of QuiG thermobarometry to estimate crystallization conditions for garnet-bearing silicic rocks.

 $\textbf{Keywords} \ \ Quartz \cdot Inclusion \cdot Garnet \cdot Experimental \cdot Barometer \cdot Thermobarometry$

Communicated by Mark S. Ghiorso.

Electronic supplementary material The online version of this article (https://doi.org/10.1007/s00410-018-1469-y) contains supplementary material, which is available to authorized users.

☑ Jay B. Thomas jthom102@syr.edu

Published online: 24 April 2018

- ¹ 204 Heroy Geology Laboratory, Department of Earth Sciences, Syracuse University, Syracuse, NY 13244, USA
- Department of Earth and Environmental Sciences, Rensselaer Polytechnic Institute, Troy, NY 12180, USA

Introduction

Minerals that contain inclusions of co-crystallizing minerals are ubiquitous in polymineralic systems. Mineral inclusion elastic thermobarometers can be developed for mineral pairs that have different elastic properties (Rosenfeld and Chase 1961; Rosenfeld 1969; Van der Molen and Van Roermund 1986; Enami et al. 2007; Ashley et al. 2014; Kohn 2014; Angel et al. 2014, 2015). At entrapment conditions, the cavity in a host mineral perfectly accommodated the volume of its inclusion, and the pressure applied to both the inclusion and host mineral were equivalent. Subsequent changes in pressure (*P*) and temperature (*T*) caused the host and inclusion volumes to change by different amounts to produce inclusions with remnant pressures (Sorby and Butler 1868). Numerous methods—including birefringence analysis, theoretical modeling, X-ray diffraction and Raman spectroscopy



measurements—have been developed to quantify remnant pressures of inclusions for thermobarometric applications (Rosenfeld and Chase 1961; Rosenfeld 1969; Adams et al. 1975a, b; Van der Molen and Van Roermund 1986; Zhang 1998; Enami et al. 2007; Howell et al. 2010; Angel et al. 2014, 2015).

Natural garnet crystals commonly contain quartz inclusions with remnant pressures that can be related to their crystallization *P*–*T* conditions. Several modeling approaches have been proposed to use remnant pressures of inclusions to estimate P-T conditions of entrapment. Because of complex inclusion-host interactions, and complicated histories of many natural samples, there has been considerable debate over appropriate approaches for elastic thermobarometry. Angel et al. (2014, 2015) demonstrated that approaches which consider only linear elastic properties of host and inclusion minerals with changes in P-T (Zhang 1998) yield inaccurate inclusion pressures. Angel et al. (2017) also showed that a model for elastic thermobarometry (Guiraud and Powell 2006) that has been widely used (Ashley et al. 2014, 2015, 2016; Kohn 2014; Spear et al. 2014) could not accurately reproduce potential entrapment conditions for most cases because of theoretical errors. Angel et al. (2017) presented a physically correct theoretical model in which inclusion pressures can be used to estimate entrapment P-Tconditions for ideal inclusion-host systems. Several correction schemes have also been proposed to adjust inclusion pressures for application of quartz-in-garnet thermobarometry (Ashley et al. 2016; Mazzucchelli et al. 2018). To date, there has been limited experimental investigation to evaluate elastic thermobarometry applications (Spear et al. 2014; Ashley et al. 2016), equation of state parameters, and correction schemes.

In this study, we performed experiments over a wide range of pressures to study how the entrapment conditions affect remnant pressures of quartz inclusions in garnet to evaluate potential usage of the quartz-in-garnet (QuiG) thermobarometer. Raman spectroscopic measurements of quartz inclusions at ambient conditions were used to calculate inclusion pressures from the 128, 206 and 464 cm⁻¹ Raman band frequencies of quartz. Inclusion pressures were used to calculate unique *P*–*T* paths, called isomekes, along which inclusions might have been trapped. The experimental run temperatures were then used to calculate entrapment pressures. The pressures measured in experiments were compared to calculated entrapment pressures to evaluate the accuracy of calculated entrapment pressures using a range of equation of state parameters for quartz and garnet. Experimental results were also used to evaluate syn- and post-entrapment modifications that might limit applications of QuiG thermobarometry.



Methods

Piston-cylinder experiments

Garnet with quartz inclusions was hydrothermally crystallized from oxide starting materials (Table 1) in piston-cylinder devices at pressures from 0.5 to 3.0 GPa and temperatures ranging from 700 to 800 °C (Table 2). Starting materials SiO₂ (amorphous), Al(OH)₃, FeO, Fe₃O₄, Fe₂O₃, FeTiO₃, and MnO (Alfa Aesar) were gently packed into silver capsules. Water was added to wet the powders completely. Seed crystals of garnet (Gore Mountain; North River, New York) were added to experiments performed at P < 2.0 GPa. Garnet crystallization required controlled oxygen fugacity. The oxygen fugacities of experiments were buffered by an assemblage of fayalite + magnetite + quartz contained in a separate adjacent capsule (Fig. 1). Approximately 15 mg of the oxide mixtures (Table 1) and $\sim 10-15$ mg H₂O were added to capsules used in the 19mm-diameter assemblies; ~10 mg of oxide mixtures and 5–8 mg H₂O were added to capsules used in the 12.7-mm-diameter assemblies (Fig. 1). It was important to leave ~ 0.75 mm of headspace in the capsules to prevent contaminating the tops of capsules with starting materials. The principle of the buffer capsule design used in these experiments (Trail et al. 2012) is identical to the principle of the classic internal capsule design (Jakobsson 2012). In our fO_2 buffered experiments tailored for piston-cylinder assemblies, platinum disks (150 µm thick) were placed between the open ends of the buffer capsules and the capsules containing the garnet-producing oxide mixture (Fig. 1). The oxygen pressure in the capsules was controlled

Table 1 Compositions of oxide mixtures used to grow garnets and control the oxygen fugacity of experiments

Oxide mixtures used	to grow garnet with quartz inclus	ions
wt% oxide	QuiG mix 1	QuiG mix 2
SiO ₂	59.23	59.12
Al_2O_3	15.39	15.37
FeO	10.10	10.08
Fe_2O_3	8.13	8.11
TiO_2	7.16	7.15
MnO	_	0.18
Fayalite-magnetite-	quartz oxygen fugacity buffer mix	ture
wt% oxide		FMQ mix
SiO ₂		23.43
FeO		38.59
Fe_3O_4		37.98

Table 2 Experimental pressure and temperature, Raman band frequency (ν), and inclusion pressure (P_{inc}) determined from Raman shift. Entrapment pressures (P_{trap}) calculated using quartz equation of state parameters for the full Landau transition model with a curved $\alpha = \beta$ quartz phase boundary model from Angel et al. (2017a), and a Tait equation of state and parameters for garnet from Holland and Powell (2011)

Expt #	Expt P (GPa)	Expt T (°C)	ν 128 (cm ⁻¹)	$\nu \ 206 \ ({\rm cm}^{-1})$	ν 464 (cm ⁻¹)	P _{inc} 128 (GPa)	P _{inc} 206 (GPa)	P _{inc} 464 (GPa)	P _{inc} average ^a (GPa)	P _{trap} (GPa)	n ₁₂₈ ^b	n ₂₀₆ ^b	n ₄₆₄ ^b
29	0.8	800	125.006 (0.135)	195.782 (0.663) ^c	462.117 (0.081)	0.2966	с	0.2948	0.2957 (0.008)	0.882	21	c	22
21	1	800	127.031 (0.098)	207.074 (0.292)	465.015 (0.067)	-0.0598	0.0384	0.0239	-0.0001 (0.008)	1.095	19	17	19
22	1	700	129.240 (0.083)	212.727 (0.309)	466.670 (0.098)	0.2437	0.2382	0.2086	0.2297 (0.007)	1.142	20	19	21
20	1.5	800	130.086 (0.155)	216.058 (0.281)	468.258 (0.121)	0.4026	0.3701	0.3880	0.3879 (0.008)	1.546	27	21	27
26	1.5	700	130.575 (0.133)	218.889 (0.180)	469.475 (0.085)	0.4666	0.4865	0.5262	0.4941 (0.007)	1.526	31	26	32
11	2	800	132.299 (0.135)	223.516 (0.811)	472.028 (0.121)	0.7424	0.6549	0.8203	0.7482 (0.016)	2.099	28	17	32
17	2	775	132.353 (0.190)	218.791 (0.551) ^c	471.878 (0.318)	0.7523	c	0.7948	0.7748 (0.022)	2.105	16	c	19
13	2	750	133.157 (0.112)	226.209 (0.322)	472.589 (0.082)	0.8973	0.8352	0.8854	0.8756 (0.009)	2.244	31	25	34
28	2	725	133.570 (0.059)	227.423 (0.231)	472.678 (0.095)	0.9690	0.8924	0.9010	0.9218 (0.007)	2.294	68	61	70
34	2.5	800	133.552 (0.078)	229.219 (0.320)	473.867 (0.129)	0.9707	0.9988	1.0351	1.0017 (0.009)	2.550	45	38	45
A-1	3	775	134.981 (0.094)	234.006 (0.312)	475.548 (0.118)	1.2511	1.2576	1.2335	1.2466 (0.010)	2.997	50	40	50

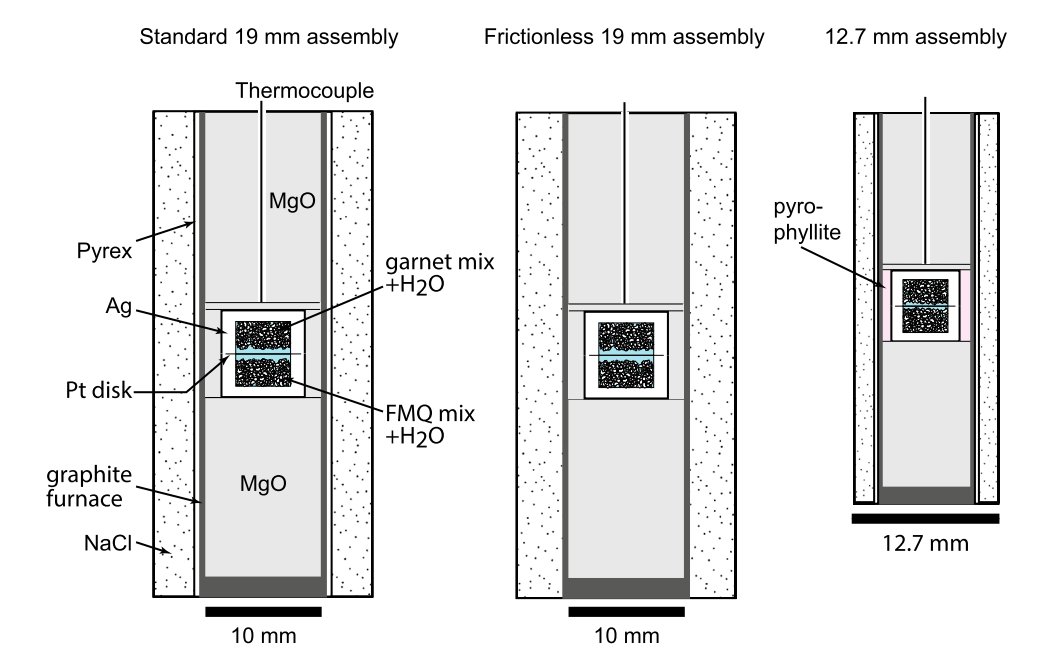
Numbers in parentheses are standard errors of the mean

^aEach Raman spectrum typically yielded three bands that were used to calculate $P_{\rm inc}$, and then $P_{\rm inc}$ values of all the bands from each experiment were used to calculate average $P_{\rm inc}$ and errors. See text for details

 $^{^{\}mathrm{b}}$ Number of measurements used to calculate P_{inc} for the subscripted Raman band frequency

 $^{^{\}rm c}$ Not used to calculate $P_{\rm inc}$ because of interference with 170 and 215 cm $^{-1}$ Raman band frequencies of garnet

Fig. 1 Assemblies used in piston–cylinder experiments



(i.e., buffered) by hydrogen diffusion across the Pt disks that separated the garnet + quartz mineral assemblages from the oxygen buffer.

The 1.0–2.0 GPa experiments were performed in 19-mmdiameter salt-pyrex-graphite assemblies that contained "squishable" MgO filler pieces (Tateho Ozark), and the 2.5-3.0 Gpa experiments were performed in 12.7-mmdiameter assemblies with similar components (Fig. 1). The 0.5 and 0.8 GPa experiments were performed in 19-mmdiameter assemblies that did not contain a Pyrex sleeve using an assembly design similar to the "frictionless" assemblies described in Holland (1980). Temperatures were monitored using type-D thermocouples (W₉₇Re₃-W₇₅Re₂₅), and are believed to be accurate to within ~5 °C. The capsules were stacked in the experimental assembly so that the capsule containing the garnet-producing mixture was on top with its closed end located < 1 mm from the thermocouple (Fig. 1). The capsule-Pt disk-capsule composite stacks were sealed during cold pressurization of each experiment. Oil pressures in the piston-cylinder hydraulic rams were measured with Enerpac 140 MPa Bourdon-tube gauges with 18-cm-diameter dials. Experiments were run for 1-4 days and quenched to below 100 °C within 20 s by turning off the furnace power.

There are potential experimental problems that could cause actual pressures in an experimental capsule to be different than pressures measured on experimental pressure gauges (Mirwald et al. 1975; Mirwald and Massonne 1980; Bose and Ganguly 1995; McDade et al. 2002). In consideration of gauge accuracy, essentially identical pressures were simultaneously measured on two pressure gauges from Enerpac[®] and three Noshok[®] pressure gauges (Supplementary Fig. S1). Additionally, numerous experiments

performed in the Syracuse University experimental lab indicate that *P*–*T* conditions measured on the piston–cylinder devices are reasonably accurate, thus, no corrections were applied to measured experimental pressures and temperatures. The quartz–coesite phase boundary was explored in another study in the Syracuse University laboratory using the same assemblies (Fig. 1) and piston–cylinder devices described here. There is good agreement between the quartz–coesite phase boundaries determined by Boyd and England (1960) and Kitahara and Kennedy (1964), and silica minerals grown along the 3.0 and 3.2 GPa isobars in our piston–cylinder devices (Supplementary Fig. S2).

The capsule—Pt disk—capsule composite stacks were opened by wrenching them apart with two pairs of pliers. Aqueous fluid was always present in both capsules at the end of experiments. Single crystals of garnet (and other minerals) were removed from capsules, mounted in epoxy and polished prior to subsequent analyses.

Analytical details

Raman spectra were measured with a Renishaw inVia Raman microprobe in the Chemistry Department at Syracuse University; some early experiments were measured with a Bruker Senterra Raman microprobe at Rensselaer Polytechnic Institute. Both instruments used incident 532 nm laser light focused onto analytical spots using $100 \times$ microscope objectives (N.A. = 0.9). Both instruments were operated in high confocality mode to maximize signal from quartz inclusions. The Raman shifted light was backscattered (180° geometry) and statically dispersed using 1800 groove/mm gratings onto charged-couple devices. Spectra were acquired



for 20-60 s. Both instruments have 0.5 cm⁻¹ spectral resolution and precision is typically < 0.1 cm⁻¹. The Renishaw spectrometer was calibrated against numerous Ne lines, and spectral accuracy and linearity were checked throughout each analytical session by measuring the Rayleigh scattered light from the 532 nm laser and the 520.5 cm⁻¹ band of a silicon standard. Over a 12-month period, repeated measurements of the Si band in a silicon metal standard material gave 520.5 ± 0.1 cm⁻¹ one standard error of the mean.

All spectra were measured at room conditions of 25 °C and 0.1 MPa. Spectra were not processed or corrected in any way prior to peak fitting using Renishaw software because the Raman spectral linearity and accuracy were stable throughout analytical sessions. Errors on fitted band positions are $\sim 0.2-0.3$ cm⁻¹, but they may be somewhat higher depending on spectral noise, peak/background ratios, and width of individual Raman band frequencies. Most measurements of quartz inclusions were performed in the outer 30–50 µm of garnet crystals, and most quartz inclusions measured were ~2-4 µm in diameter. The frequencies of the three main Raman bands in quartz at 127.9, 205.9 and 464.8 cm^{-1} are generally referred to as the 128, 206 and 464 bands.

Major element compositions of garnets were measured at Syracuse University with a Cameca SXFive using a 20 nA beam and 15 kV accelerating voltage. A field emission scanning electron microscope (Carl Zeiss Supra) at Rensselaer Polytechnic Institute was used to image the experimental run products. Secondary and backscattered electron images were acquired using 5-20 kV accelerating voltage.

(a)

P=2.0 GPa

P=1.0 GPa

T=700°C $P_{11} = 0.209 \text{ GPa}$

(b)

T=800°C P_{inc}=0.820 GPa

473.1

Fig. 2 Transmitted light micrographs of experimentally grown garnet with quartz inclusions. a Two almandine crystals typical of those that spontaneously nucleated at $P \ge 2$ GPa, **b.** c almandine composition rims overgrown on garnet seed crystals; d spessartine-rich rim overgrown on a garnet seed crystal. Numbers denote the observed Raman frequency of the 464 cm⁻¹ band of the quartz inclusions. Pressures listed were calculated for the 464 cm⁻¹ band

plementary Table S1). All other P-T conditions required addition of seed garnet crystals to grow garnet. The garnets grew as mantles on seed crystals, and completely new crystals also nucleated. In experiments performed at P < 1.0 GPa the seed crystals were consumed during the runs; addition (c) 50 μm 472.2 472.4 *P*=1.0 GPa P_{inc} =24 MPa (d) 462.0 466.9

462.2

P=0.8 GPa T=800°C

466.6

Results and discussion

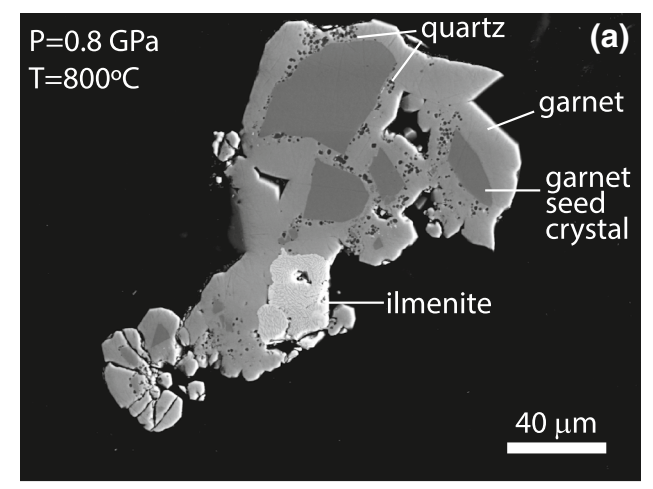
Equant and well-faceted garnet crystals with maximum dimensions up to ~200 µm (Figs. 2, 3) crystallized with quartz, an aluminosilicate (kyanite at $P \ge 1.5$; sillimanite at P < 1.5 GPa), staurolite, chloritoid, ilmenite and rutile in the experiments. Quartz inclusions in garnet formed in all experiments up to 800 °C; at higher T, quartz inclusions did not form. The garnet crystals have sieve textures with inclusions of all the co-crystallizing minerals (Figs. 2, 3). The quartz inclusions range from sub-micrometer spherical inclusions to well-faceted inclusions 30 µm in maximum dimension (Fig. 2b). The quartz inclusions in the 700 °C experiments are significantly smaller than inclusions in higher temperature experiments. Experiments performed at T<700 °C yielded quartz inclusions that were too small to measure individually with our Raman systems. In the seeded experiments, quartz inclusions were preferentially trapped near the interface between the seed crystal and the garnet grown in the experiment (Figs. 2, 3).

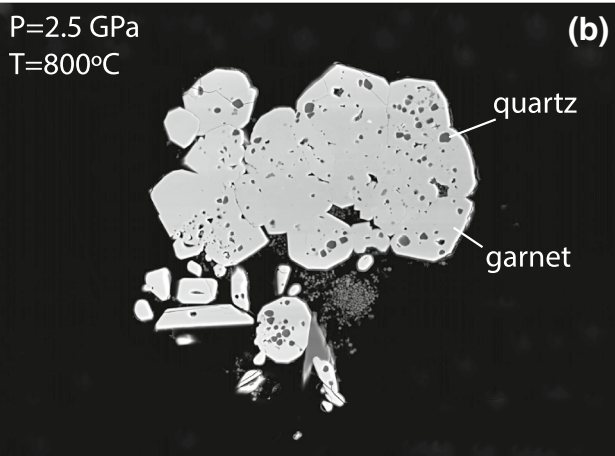
Garnet spontaneously nucleated from the QuiG mix #1 bulk composition (Table 1) at $P \ge 2.0$ GPa to crystallize garnet crystals with compositions > 99% almandine (Sup-



garnet crystal

464. 462.1





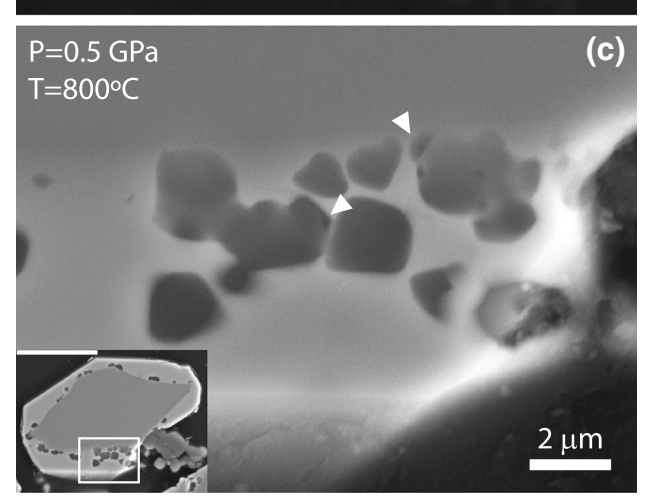
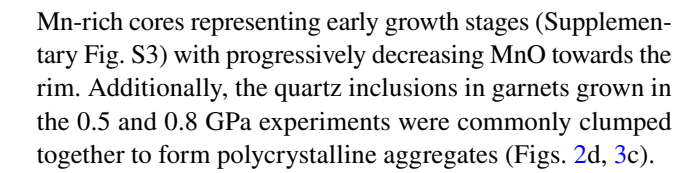


Fig. 3 Backscattered electron images of garnets from experiments performed at **a** 0.8 GPa and 800 °C; **b** 2.5 GPa and 800 °C. **c** Secondary electron images of garnet from an experiment performed 0.5 GPa and 800 °C. Arrows denote dilatational features formed at inclusion—host interfaces. Scale bar in inset is 20 μ m

of MnO was required to stabilize garnet seeds and initiate new garnet growth. Similar to observations in some natural metamorphic rocks, the experimental garnet crystals have



Raman measurements of quartz inclusions in garnet

The average frequencies for the 128, 206 and 464 cm⁻¹ Raman bands in quartz inclusions are listed in Table 2 and shown in Fig. 4a. A round quartz inclusion 8 µm in diameter was used as a reference material. Repeat measurements (n = 41) of the 128, 206 and 464 cm⁻¹ bands in the reference quartz inclusion have ranges of 0.742, 2.762 and 1.283 cm⁻¹, and standard errors of the mean are 0.032, 0.096 and 0.030 cm⁻¹. For measurements of experimental specimens, single spectra were typically measured on inclusions contained in multiple crystals (Fig. 2). Intracrystalline and intercrystalline variations of band positions of quartz inclusions from individual experiments were small. Most inclusions in our experimental garnets are smaller than the inclusion used as a reference material. For this reason, spectra may be of lower quality and band positions may have larger errors. The standard errors of the mean for the 128, 206 and 464 cm⁻¹ bands from individual experiments are smaller than 0.19, 0.82 and 0.32 cm⁻¹, respectively (Table 2). The 206 cm⁻¹ band of unencapsulated quartz (~23 cm⁻¹ full width at half maximum; FWHM) is significantly wider than the 128 and 464 cm $^{-1}$ bands ($< 10 \text{ cm}^{-1}$ FWHM). For quartz inclusions in garnet, spectral interferences from the ~170 and 215 cm⁻¹ Raman band frequencies of garnet (Fig. 4a) occur in close proximity to the 206 cm⁻¹ frequency of quartz and may cause linewidth broadening of the 206 cm⁻¹ band (Fig. 4a). Both factors complicate usage of the 206 cm⁻¹ band to determine $P_{\rm inc}$ for quartz inclusions in garnet, and contribute to the lower precision for the 206 cm⁻¹ frequency compared to the 128 and 464 cm⁻¹ bands (Fig. 4a; Table 2).

The pressures of quartz inclusions ($P_{\rm inc}$) in garnet were calculated from Raman spectroscopic measurements performed at 25 °C. The 128, 206 and 464 cm⁻¹ Raman band frequencies systematically change with pressure and temperature (Dean et al. 1982; Hemley 1987; Liu and Mernagh 1992; Schmidt and Ziemann 2000; Enami et al. 2007). All calibrations that describe the P-T dependencies of Raman band shifts were determined for quartz under hydrostatic pressure. Over the range of experimental pressures, the 128, 206 and 464 cm⁻¹ Raman band frequencies measured in quartz inclusions from our experiments were shifted by 11, 24, and 14 cm⁻¹ (Fig. 4a; Table 2).

Equations and data in Schmidt and Ziemann (2000) that describe the pressure dependencies of the 206 and 464 cm⁻¹ bands were used to calculate quartz P_{inc} from Raman band positions listed in Table 2. They did



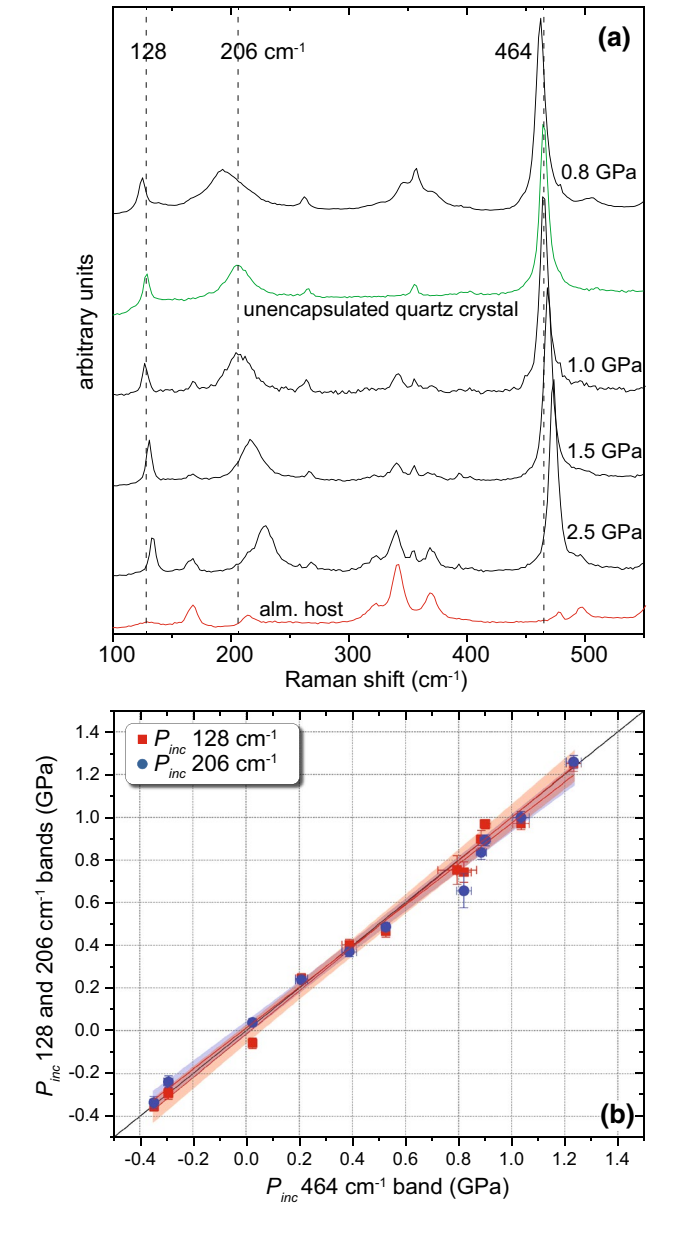


Fig. 4 a Raman spectra of quartz inclusions trapped in garnets. The 128, 206 and 464 cm⁻¹ frequencies of quartz inclusions systematically change with experimental pressure. The dashed lines are the Raman band frequencies of unencapsulated quartz crystals. Note that signal from the host almandine crystals is present in all inclusion spectra. **b** Inclusion pressures ($P_{\rm inc}$) calculated for the 128 and 206 cm⁻¹ Raman band frequencies of quartz inclusions plotted against $P_{\rm inc}$ calculated from the 464 cm⁻¹ band frequencies. Error bars are two standard errors of the mean. Colored bands are the 95% confidence interval for linear fits to the data that considered errors in x and y. The black diagonal line is the 1:1 correlation. See text for details

not give an equation for the pressure dependence of the 128 cm^{-1} frequency. To calculate P_{inc} from shifts of the 128 cm^{-1} bands, we fit a polynomial to the data presented in Schmidt and Ziemann's Fig. 2 to obtain

P (GPa) = 0.13143 (±0.00296) Δv + 0.00475 (±3.1561E – 4) Δv^2 in which Δv is the difference between the measured frequency of quartz under pressure and that of unencapsulated quartz crystals (C. Schmidt provided the 128 cm⁻¹ band data via personal communication).

Each Raman spectrum typically yielded three bands that were used to calculate $P_{\rm inc}$, and then $P_{\rm inc}$ values of all the bands from each experiment were used to calculate average $P_{\rm inc}$ and errors at the 95% confidence interval (Fig. 4b; Table 2). Inclusion pressures determined from the 128, 206 and 464 cm⁻¹ bands are not statistically different from one another. Linear fits to $P_{\rm inc}$ calculated from the 464 and 128 cm⁻¹ bands, and from the 464 and 206 cm⁻¹ bands have 95% confidence bands that significantly overlap one another, and confidence intervals from both fits overlap perfect 1:1 correlations (Fig. 4b). Because pressures calculated from the three Raman bands are similar, we report $P_{\rm inc}$ calculated from averages of the 128, 206 and 464 cm⁻¹ Raman band frequencies (Table 2). Negative frequency shifts, relative to unencapsulated quartz, measured for quartz inclusions in garnet from experiments performed at 0.5 and 0.8 GPa give negative $P_{\rm inc}$ for each of the Raman bands. Average $P_{\rm inc}$ values range from -0.351 to 1.247 GPa (Table 2). At a given pressure, inclusions trapped in garnet grown at lower temperature have higher pressures. The experimental quartz inclusions have $P_{\rm inc}$ values (Fig. 4b) that essentially span the entire range of $P_{\rm inc}$ values observed in quartz inclusions in garnets from natural rocks (Enami et al. 2007; Kouketsu et al. 2014; Ashley et al. 2015; Castro and Spear 2016).

The 464 cm⁻¹ band of quartz is significantly more intense than the 128 and 206 cm⁻¹ bands (Fig. 4a). Because the 128 cm⁻¹ band is pleochroic, the band was not present in spectra of quartz inclusions in some orientations (Table 2). Usage of the 206 cm⁻¹ band of quartz inclusions to determine $P_{\rm inc}$ is complicated because the band is relatively wider, and it contains spectral contributions from the garnet hosts (Fig. 4a). Spectral contributions from the garnet hosts to the quartz 206 cm⁻¹ band are dependent upon the amount of host included within the analytical volume. Because of difficulties deconvolving spectral interferences, the 206 cm⁻¹ Raman band was not used to calculate average $P_{\rm inc}$ for inclusions from experiments #17 and #29 (Table 2). In many other cases insufficient peak-to-background ratios, pleochroism, and linewidth broadening caused by spectral interferences forbade use of the 128 and 206 cm⁻¹ bands (see last columns in Table 2). We emphasize that usage of any of the individual Raman bands would not change foregoing conclusions. Additionally, the practical limitations of performing confocal measurements of small quartz inclusions in a garnet should be borne in mind; the quality of spectra from 1 to 2 µm diameter inclusions are lower than that of larger inclusions. In most cases, Raman band position errors of ~ 0.3 cm⁻¹ can cause the observed discordancy



amongst $P_{\rm inc}$ values calculated from each of the Raman band frequencies, which is similar to the accuracy of spectral fits to the individual bands. Because $P_{\rm inc}$ values calculated from each of the bands give essentially the same result (Fig. 4b), the more intense 464 cm⁻¹ band can be used without necessarily considering the 128 and 206 cm⁻¹ bands that may be more difficult to measure accurately.

Comparison of experimental *P–T* conditions to calculated entrapment pressures

When quartz and garnet were co-crystallizing in the experimental system prior to entrapment the pressure applied to quartz must have been the same as that applied to the garnet crystals. In our experiments quartz and garnet were crystallizing into free space inside the capsules from quartz- and garnet-saturated aqueous fluids, thus they were subjected to hydrostatic pressures. For elastically isotropic inclusion-host systems, when a crystal is trapped as an inclusion in a host, the cavity in the host perfectly accommodated the inclusion, which means that the external pressure applied to the host crystal was the same as that applied to the inclusion (see square-shaped symbols in Fig. 5a). After entrapment of an inclusion there is a single P-T path, called an entrapment isomeke, along which the fractional volume change of host and inclusion were equivalent (Rosenfeld and Chase 1961; Adams et al. 1975a, b; Angel et al. 2014, 2015, 2017b). At all points along an isomeke an inclusion perfectly filled its cavity and no stresses developed in the inclusion-host system—the pressure in the inclusion was the same as that applied to the garnet. In other words, isomekes define the P-T points along which inclusions with a specific P_{inc} could have been entrapped (Fig. 5a). Pressure in an inclusion that is different from that imposed on the host mineral will develop when the P-T conditions change along a path that is not coincident with the entrapment isomeke.

Angel et al. (2014, 2015, 2017b) gave an exact solution for modeling pressure development in mineral inclusions. Average $P_{\rm inc}$ determined from all three Raman band frequencies (Table 2) were used to calculate isomekes using the publically available EosFit-Pinc module (http://www.rossangel.com/home.htm). Changes in the inclusion pressure from entrapment to ambient conditions were calculated using the relation:

$$P_{\text{inc}} = P_{\text{end}} - \frac{4\mu}{3} \frac{V_{P \text{ trap}}^{i}}{V_{P \text{ foot}}^{i}} \left(\frac{V_{P \text{ end}}^{h}}{V_{P \text{ trap}}^{h}} - \frac{V_{P \text{ inc}}^{i}}{V_{P \text{ trap}}^{i}} \right)$$
(1)

(Angel et al. 2017, their Eq. A6), where $P_{\rm end}$ is the pressure at which the Raman shift was measured; μ is the shear modulus of the garnet host; $P_{\rm foot}$ is the pressure where the isomeke intersects the temperature of Raman measurements;

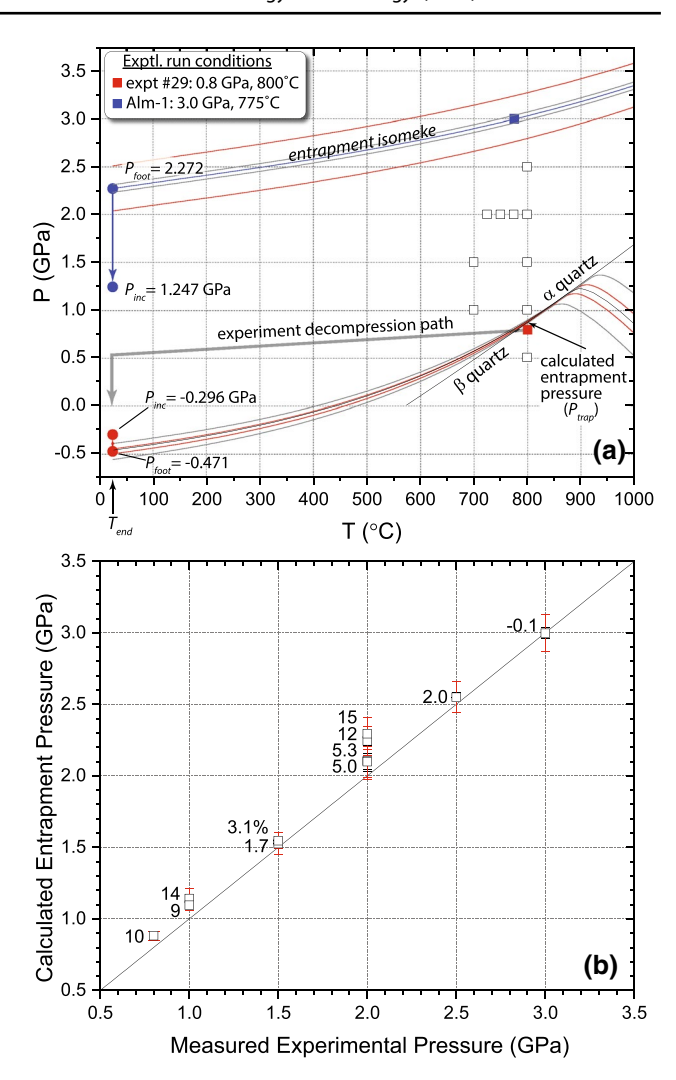


Fig. 5 a Experimental run conditions (squares) compared to calculated P_{trap} for experiments #29 and A-1 (Table 2). Entrapment isomekes were calculated using average inclusion pressures (P_{inc}) and Eq. 1. For clarity, isomekes of experimental conditions represented by open symbols are not shown. The experimental decompression path was measured during an experimental quench. The red colored isomekes show the errors from a ± 0.5 cm⁻¹ error on Raman measurements; gray isomekes show two standard errors of the mean. The curved $\alpha = \beta$ phase boundary is from Angel et al. (2017a). **b** Measured experimental pressures compared to average calculated entrapment pressures. Numbers next to symbols are the percent difference between measured experimental pressures and calculated entrapment pressures. Black error bars are two standard errors of the mean (mostly smaller than symbols), and red error bars represent ± 0.5 cm⁻¹ error on Raman measurements. The black diagonal line is the 1:1 correlation. See text for details

 $P_{\rm trap}$ is the pressure at which the inclusion was trapped in the host and $V^{\rm h}$ and $V^{\rm i}$ refer to the volumes of the host and inclusion at the subscripted conditions. As described above, inclusion pressures were determined from Raman frequency shifts in quartz inclusions that were measured at $P_{\rm end}$ (0.1 MPa) and $T_{\rm end}$ (25 °C), and μ is the shear modulus of garnet (Wang and Ji 2001). Quartz volumes were



calculated using a P–T–V equation of state and parameters for the full Landau transition and curved $\alpha = \beta$ phase boundary model (Angel et al. 2017a, b). Garnet volumes were calculated using Birch–Murnaghan and Tait equations of state described in Holland and Powell (2004, 2011) and equation of state parameters from references listed in Table 3. The reader is referred to Angel et al. (2017) for details on the theory and methodology.

Isomekes of quartz inclusions in garnet have relatively flat slopes so they are best used as a geobarometer. The $P_{\rm inc}$ values from our experiments were used to define entrapment isomekes along which inclusions could have been trapped, and then calculated $P_{\rm trap}$ was determined from the entrapment isomeke at the measured experimental temperatures (Fig. 5a; Table 2).

Accuracy of calculated entrapment pressures

The accuracy of QuiG geobarometry can be evaluated by considering the differences between measured experimental pressures and calculated $P_{\rm trap}$ using published thermodynamic parameters and equations of state (Fig. 5b). Table 3 lists $P_{\rm trap}$ calculated using almandine parameters that span

the range of published values, and two equation of state models for quartz. The closest agreement between calculated $P_{\rm trap}$ and measured experimental pressures (Fig. 5b) are for calculations that used the equation of state parameters for quartz that employs the full Landau transition and a curved $\alpha = \beta$ phase boundary (Angel et al. 2017a), and equation of state parameters for almandine and spessartine listed in Holland and Powell (2011); host garnet parameters listed in Zhang et al. (1999) give similar results (Table 3). Calculated $P_{\rm trap}$ are remarkably similar to the pressures measured during the experiments, but they are systematically higher than measured experimental pressures (Fig. 5b). In general, discrepancies between calculated P_{trap} and measured experimental pressures are largest for the lower pressure experiments. For example, the experiments at 0.8, 2.5 and 3.0 GPa were 10, 2 and -0.1% from the measured experimental pressure, respectively (Fig. 5b). Most experiments have calculated $P_{\rm trap}$ that are less than ~ 10% different from the experimental pressure. For comparison, conventional thermobarometric methods based on calculation of equilibrium constants from measured mineral compositions, activity models, and thermodynamic data give P estimates with uncertainties that

Table 3 Accuracy of calculated entrapment pressures (P_{trap}) relative to measured experimental pressures. The models used published equation of state parameters for quartz and garnet. Numbers in parentheses are the percentage differences from measured experimental pressures

Expt. #	Measured P (GPa)	Calculated entrapment pressures								
		Model 1 ^a P (GPa)	Model 2 ^a P (GPa)	Model 3 ^a P (GPa)	Model 4 ^a P (GPa)	Model 5 ^a P (GPa)	Model 6 ^d P (GPa)			
29 ^b	0.8	0.882 ^b (10.3)	0.882 ^b (10.3)	0.882° (10.3)	N/A	N/A	0.951 ^b (18.9)			
21	1	1.095 (9.5)	1.108 (10.8)	1.097 (9.7)	1.141 (14.1)	1.114 (11.4)	1.141 (14.1)			
22	1	1.142 (14.6)	1.113 (11.3)	1.146 (14.6)	1.203 (20.3)	1.171 (17.1)	1.169 (16.9)			
20	1.5	1.546 (3.1)	1.548 (3.2)	1.552 (3.5)	1.627 (8.5)	1.591 (6.1)	1.551 (3.4)			
26	1.5	1.526 (1.7)	1.576 (5.1)	1.535 (2.3)	1.610 (7.3)	1.577 (5.1)	1.523 (1.5)			
11	2	2.099 (5)	2.222 (11.1)	2.114 (5.7)	2.217 (10.9)	2.179 (8.9)	2.042 (2.1)			
17	2	2.105 (5.3)	2.138 (6.9)	2.12 (6.0)	2.223 (11.2)	2.186 (9.3)	2.044 (2.2)			
13	2	2.244 (12.2)	2.263 (13.2)	2.261 (13.1)	2.37 (18.5)	2.336 (16.8)	2.167 (8.3)			
28	2	2.294 (14.7)	2.255 (12.8)	2.313 (15.7)	2.423 (21.2)	2.392 (19.6)	2.209 (10.5)			
34	2.5	2.55 (2.0)	2.613 (4.5)	2.572 (2.9)	2.699 (8.0)	2.662 (6.5)	2.433 (-2.7)			
A-1	3	2.997 (-0.1)	2.968 (-1.1)	3.027 (0.9)	3.171 (5.7)	3.143 (4.8)	2.819 (-6)			

^aModels 1–5, quartz equation of state parameters for the full Landau transition model with a curved $\alpha = \beta$ quartz phase boundary model from Angel et al. (2017a)

Model 4, almandine values from Milani et al. (2015)

Model 5, almandine values from Yagii et al. (1987)

^dModel 6, quartz equation of state parameters for the "simple" equation of state from Angel et al. (2017a) that has a linear $\alpha = \beta$ quartz phase boundary and considers elastic softening only in α quartz; almandine and spessartine values from Holland and Powell (2011)



^bModel 1, almandine and spessartine values from Holland and Powell (2011)

^bModel 2, P_{inc} values used to calculate P_{trap} determined from the quartz 464 cm⁻¹ band only. Almandine and spessartine values from Holland and Powell (2011)

^cModel 3, almandine and spessartine values from Zhang et al. (1999)

42

are significantly higher than 10% (Kohn and Spear 1991a, b; Worley 2000; Powell and Holland 2008).

Calculations of $P_{\rm trap}$ using other equation of state parameters for quartz and garnet have larger discrepancies (Table 3). A simplified equation of state model for quartz (Angel et al. 2017a) that considers elastic softening only in β quartz and a linear phase boundary yields $P_{\rm trap}$ that are significantly higher than measured experimental pressures. Also, elastic parameters that produce relatively 'softer' almandine give higher entrapment pressures (Table 3).

Potential sources of error in elastic thermobarometry

The experiments provide an opportunity to explore potential problems that may limit usage of quartz inclusions in garnets to estimate *P*–*T* conditions of garnet crystallization. The physical model that describes volumetric changes that produce remnant pressures in inclusions (Eq. 1) is necessarily simple so that routine calculations are possible. All models assume that inclusions are small compared to the host, spherical in shape, and that inclusion-host systems are elastically isotropic. In many real inclusion-host systems—such as quartz in garnet—none of the physical model requirements is strictly true. Additionally, equations that describe the pressure dependencies of the three main Raman bands commonly used to calculate quartz $P_{\rm inc}$ (e.g., Schmidt and Ziemann 2000) are applicable to quartz under hydrostatic pressure. Because quartz is elastically anisotropic and garnet is nearly elastically isotropic, non-hydrostatic stresses must develop in quartz inclusions in garnet. We make some first-order observations on the magnitude of effects caused by non-ideal inclusion characteristics on calculated entrapment conditions, and evaluate the accuracy of using Raman measurements performed at 25 °C and mineral equations of state to estimate $P_{\rm inc}$ and $P_{\rm trap}$.

Estimating $P_{\rm trap}$ from room temperature measurements

Ashley et al. (2016) provided a generic and empirical scheme to calculate $P_{\rm trap}$. They suggested that when possible $P_{\rm inc}$ should be determined from Raman measurements performed at estimated formation temperatures to determine $P_{\rm trap}$. In the absence of heating experiments and high-temperature measurements, Ashley et al. (2016) suggested that $P_{\rm trap}$ could be determined as follows: (1) estimate entrapment temperature, (2) calculate $P_{\rm trap}$ from $P_{\rm inc}$ determined at 25 °C, (3) interpolate between heating data linear regressions (their Fig. 3) to obtain the slope and intercept of a line that passes through the estimated formation temperature from step 1, and (4) estimate a "corrected" formation pressure from the fitted line and the estimated temperature from

step 1. Applying the proposed correction scheme to experiments #26 and #20 that have calculated entrapment pressures of 1.526 and 1.546 GPa (Table 2) gives interpolated slopes of ~ -0.46 MPa/°C. Using the measured experimental temperatures gives "corrected" entrapment pressures of ~ 1.05 GPa, which significantly underestimates the 1.5 GPa experimental pressure. The adjustment scheme of Ashley et al. (2016) underestimates entrapment pressures by $\sim 30\%$.

Syn-entrapment modifications to inclusion pressures (P_{inc})

Numerous syn-entrapment modifications could affect quartz inclusions in garnet to yield $P_{\rm inc}$ values closer to those of unencapsulated quartz. Mazzucchelli et al. (2018) used finite-element methods to model geometric effects on the stress state of inclusion—host systems (i.e., $P_{\rm inc}$). For 'soft' inclusions in 'stiff' hosts, like quartz in garnet, geometric effects can cause the pressure in a non-ideal inclusion to be significantly lower than the pressure in an ideal inclusion formed at the same conditions. Specifically, Mazzucchelli et al. (2018) considered syn-entrapment geometric effects on $P_{\rm inc}$ caused by relatively large inclusions (compared to the host), nonspherical shaped inclusions, and inclusion proximity to an interface (e.g., grain boundaries, cracks, etc.). They provided methods (their Fig. 2 and 3) to correct for non-ideal geometries using the relation $P_{\rm inc}^{\rm corrected} = \frac{P_{\rm inc}^{\rm non-ideal}}{1+\Gamma}$, in which $P_{\rm inc}^{\rm non-ideal}$

is inclusion pressure of a geometrically compromised inclusion, and Γ is a geometric factor for an inclusion's relative size, its proximity to an interface, and the shape of an inclusion. All Γ values for quartz in garnet are negative.

Most quartz inclusions measured in our experiments were 2–4 μm in diameter and contained in garnet hosts > 100 μm in diameter. Quartz inclusions that were located within < 5 µm beneath the polished garnet surfaces were usually cracked or had deformation-induced interference fringes observable with a petrographic microscope, thus they were not used to calculate isomekes; inclusions used to calculate isomekes were located > 10 µm beneath polished surfaces. Measured inclusions had approximately spherical shapes with maximum aspect ratios of 1:1:1.2. Size, proximity and shape measurements of our specimens indicate that summed Γ values are essentially zero, and geometric corrections were not required for application of elastic thermobarometry to our specimens. Because all possible Γ values for quartz in garnet are negative (Mazzucchelli et al. 2018), applying a geometric correction to our results would increase P_{inc} values, and calculated P_{trap} would be higher than shown in Fig. 5b.



Post-entrapment modifications to inclusion pressures (P_{inc})

Post-entrapment modifications such as cracking and deformation of the inclusion-host system (brittle or plastic) could obviously relieve remnant pressures of inclusions. Many studies have observed that exposed and/or cracked inclusions contain remnant pressures despite breaching (Sorby and Butler 1868; Korsakov et al. 2009; Zhukov and Korsakov 2015; Avadanii 2017). The Raman band frequencies of cracked and/or exposed quartz inclusions in our specimens are always less than unexposed inclusions, but the inclusions do not typically attain frequencies of unencapsulated quartz crystals (Supplementary Fig. S4). Exposed quartz inclusions in garnet with Raman frequencies most similar to unencapsulated quartz are ones that were significantly thinned by grinding/polishing; inclusions that were barely exposed have frequencies more similar to fully encapsulated quartz inclusions. As such, there is typically a large range of Raman frequency shifts observed for cracked inclusions and inclusions exposed at a polished surface (Supplementary Fig. S4).

The P-T dependencies of Raman band frequency shifts have not been calibrated at negative pressures. Models that describe the pressure dependencies of the Raman band frequencies used to calculate quartz $P_{\rm inc}$ were calibrated for positive Raman shifts produced by a hydrostatic pressure medium (Schmidt and Ziemann 2000). The accuracy of pressures calculated from negative frequency shifts must be considered with caution. Nevertheless, in order for an inclusion to faithfully retain negative remnant pressures requires that the inclusion remain perfectly attached to its host cavity walls when tensional stresses develop during cooling (Van der Molen and Van Roermund 1986; Kouketsu et al. 2014; Ashley et al. 2015).

Calculations using the experimental decompression path in Fig. 5a show that when the 0.8 GPa experiment (#29; Table 2) cooled to <315 °C, tensional forces developed negative pressures in the inclusions. There is no microscopic evidence that inclusions from the experiment detached from the inclusion-cavity walls, but it is conceivable that the difference between measured experimental pressure and calculated $P_{\rm trap}$ may be attributed to limited detachment of inclusions from the walls of host minerals. The inclusions have $P_{\rm inc} = -0.296$ GPa, that when projected back to entrapment conditions, overestimates the experimental run condition by ~10% (Fig. 5a, b; Table 3). Calculations show that a $P_{\rm inc}$ value of -0.452 GPa would be required to produce an isomeke that intersects the experimental condition.

Inclusions trapped in experiments performed at 0.5 GPa and 800 °C have dilatational features indicating detachment from inclusion-cavity walls must have been caused by tensional stresses. Most inclusions exposed on the polished surfaces have void spaces at the inclusion-host interface

(Fig. 3c). Because there is evidence for inclusion detachment from the inclusion-cavity walls, results from this experiment were not used to calculate an isomeke. Average $P_{\rm inc}$ values of -0.377 GPa indicate strong tensional forces are acting on inclusions, but $P_{\rm inc}$ values are not as low as predicted based on the isomeke that intersects the run condition. Calculations show that a $P_{\rm inc}$ value of -0.520 GPa would be required to produce an isomeke that intersects the experimental condition. Ashley et al. (2016) showed that -444 MPa was retained in an inclusion during heating and cooling experiments, which means that some inclusions can retain more negative pressures than observed here. The pressure in our experiments decreased in response to cooling, and pressure was relieved when the experiment was at room temperature (Fig. 5a). To some extent, the degree of inclusion detachment from the walls of the host must be controlled by the cooling *P*–*T*–*t* path in experimental and natural systems. It is likely that $P_{\rm inc}$ values of approximately -0.3 GPa represent the lower limit for which inclusions from our experiments can be reliably used to estimate P_{trap} .

Syn- and post-entrapment modifications cannot explain calculated $P_{\rm trap}$ that are systematically higher than pressures measured during experiments for any of the inclusions that have positive $P_{\rm inc}$ values because all recognized modifications would serve to lower $P_{\rm inc}$, which would cause $P_{\rm trap}$ to be underestimated. Likewise, experimental problems related to friction in piston–cylinder experiments (e.g., McDade et al. 2002) would cause lower $P_{\rm inc}$ and $P_{\rm trap}$ values. For an experiment to have $P_{\rm trap}$ higher than experimentally measured pressures means that $P_{\rm inc}$ values determined from Raman measurements must be higher than theoretically expected, which would give higher pressure at $P_{\rm foot}$ and thus higher $P_{\rm trap}$ (Fig. 5a).

Discrepancies between measured experimental pressures and calculated P_{trap} likely result from a combination of errors in experimental \dot{P} -T conditions, Raman measurements, spectral fitting, equations of state parameters, and potential errors in using hydrostatic pressure calibrations for Raman band positions to calculate P_{inc} of quartz inclusions in garnet. The potential effects of hydroxyl on elastic properties of quartz and garnet are not well constrained. Systematic errors on pressure measurements are possible, but it is unlikely that similar systematic errors would occur on all gauges from two manufacturers (Supplementary Fig. S1) across the range of pressures studied. Additionally, the quartz-coesite phase boundary from two experimental studies bracket our results (Supplementary Fig. S2). One potentially relatively large source of error is from Raman measurements. As discussed above and shown in Fig. 5a, small inaccuracies on Raman band positions will yield large errors in $P_{\rm inc}$, which translate to increasingly erroneous P_{trap} values with increasing pressure. For example, a 0.5 cm⁻¹ error on Raman band frequencies of quartz inclusions trapped in the 0.8 GPa experiment



42

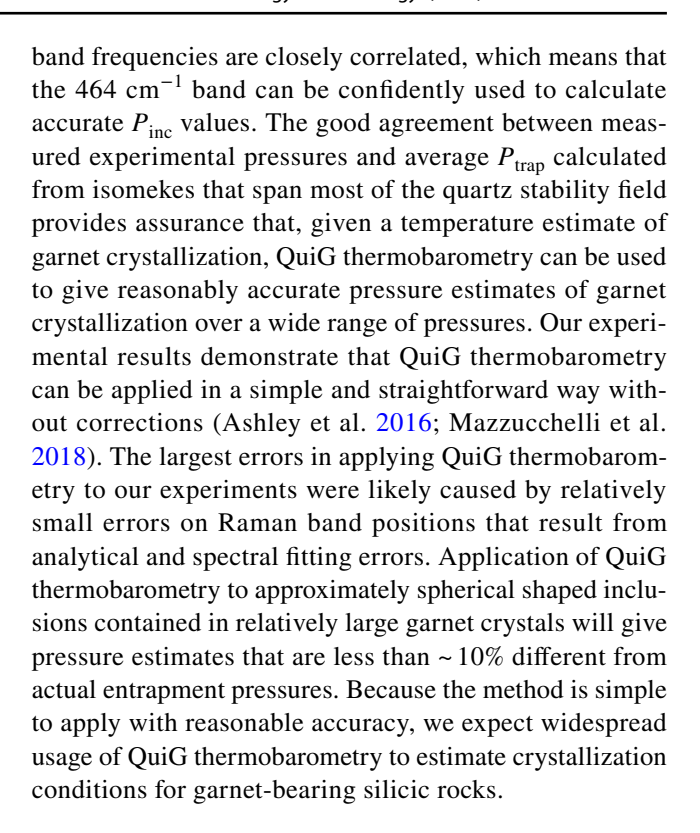
gives an error on $P_{\rm inc}$ of ~54 MPa, which translates to an error on $P_{\rm trap}$ of ~20 MPa (Fig. 5a, b). A 0.5 cm⁻¹ error on Raman band frequencies of quartz inclusions trapped in the 3 GPa experiment gives an error on $P_{\rm inc}$ of ~63 MPa, which translates to an error on $P_{\rm tran}$ of ~130 MPa.

After a quartz inclusion is enclosed as an inclusion, isotropic strains from garnet hosts are imposed on elastically anisotropic quartz, and deviatoric stress must affect the stress state of quartz inclusions (Angel et al. 2014; Mazzucchelli et al. 2018). Electron-backscatter diffraction measurements of exposed quartz inclusions from our experiment at 2.0 GPa and 800 °C (Avadanii 2017) show evidence for measureable deviatoric stresses around quartz inclusions in garnet. It is conceivable that Raman bands with phonon polarizations parallel to the c axis (the pleochroic E mode at 128 cm⁻¹) and phonons with polarization perpendicular to the c axis (A modes at 206 and 464 cm⁻¹; Zhang and Scott 2007) may respond to deviatoric stresses. The magnitude of deviatoric stress effects on P_{inc} values calculated from Raman spectroscopy has not yet been determined. However, the close agreement of P_{inc} values determined from unpolarized Raman measurements of the 128, 206 and 464 cm⁻¹ bands in quartz (Fig. 4b), and the good agreement between experimentally measured pressures and calculated P_{trap} values suggests that deviatoric stress effects are probably less than ~ 10%.

It will be challenging to discriminate Raman measurement errors on band positions and resultant P_{inc} values from potential effects caused by elastic anisotropy and deviatoric stresses. For a quartz inclusion in garnet with $P_{\rm inc}$ of 0.5 GPa, a relatively small $+0.3 \text{ cm}^{-1}$ error on the 128, 206 and 464 cm^{-1} band positions would give P_{inc} values of 0.550, 0.513 and 0.534 GPa, which could be mistaken for elastic anisotropy. There will likely be continued reliance on Raman spectroscopy to determine $P_{\rm inc}$ because other potential analytical methods that could measure the actual stress state of inclusions do not currently have sufficient spatial resolution to measure quartz inclusions in garnet that are typically smaller than ~30 µm in diameter. Our Raman measurements show that calibrations for hydrostatic pressure dependencies of quartz Raman bands (Schmidt and Ziemann 2000) can be used to calculate $P_{\rm inc}$ values of inclusions without causing significant errors in applications of QuiG thermobarometry.

Conclusions

The range of $P_{\rm inc}$ values observed in quartz inclusions in garnet from the experiments are similar to the range of $P_{\rm inc}$ values found in natural rocks. Our results show that hydrostatic pressure calibrations for the three main Raman bands in quartz from Schmidt and Ziemann (2000) give essentially the same $P_{\rm inc}$ values. Within analytical uncertainties, $P_{\rm inc}$ calculated for each of the three Raman



Acknowledgements This work was supported by the Earth Sciences Division of the National Science Foundation through grant number EAR-1447468. JT thanks David Adams, Guiomar Camano and Anthony Crespo for assistance on numerous experiments, and Tara Kahan for usage of the Renishaw Raman Spectrometer. Numerous discussions with Mattia Bonazzi, Mateo Alvaro and Ross Angel greatly improved our understanding of inclusions with remnant pressures. Formal reviews by Matthew Kohn, Fabrizio Nestola and an anonymous reviewer greatly improved the final version of the manuscript.

References

Adams HG, Cohen LH, Rosenfeld JL (1975a) Solid inclusion piezothermometry I: comparison dilatometry. Am Mineral 60:574–583 Adams HG, Cohen LH, Rosenfeld JL (1975b) Solid inclusion piezothermometry II: geometric basis, calibration for the association quartz-garnet, and application to some pelitic schists. Am Mineral 60:584–598

Angel RJ, Mazzucchelli ML, Alvaro M et al (2014) Geobarometry from host-inclusion systems: the role of elastic relaxation. Am Mineral 99:2146–2149. https://doi.org/10.2138/am-2014-5047

Angel RJ, Nimis P, Mazzucchelli ML et al (2015) How large are departures from lithostatic pressure? Constraints from host-inclusion elasticity. J Metamorph Geol 33:801–813. https://doi.org/10.1111/jmg.12138

Angel RJ, Alvaro M, Miletich R, Nestola F (2017a) A simple and generalised P–T–V EoS for continuous phase transitions, implemented in EosFit and applied to quartz. Contrib Mineral Petrol. https://doi.org/10.1007/s00410-017-1349-x

Angel RJ, Mazzucchelli ML, Alvaro M, Nestola F (2017b) EosFit-Pinc: a simple GUI for host-inclusion elastic thermobarometry. Am Mineral 102:1957–1960. https://doi.org/10.2138/am-2017-6190



- Ashley KT, Caddick MJ, Steele-MacInnis MJ et al (2014) Geothermobarometric history of subduction recorded by quartz inclusions in garnet: quartz inclusion barometry. Geochem Geophys Geosyst 15:350–360. https://doi.org/10.1002/2013GC005106
- Ashley KT, Darling RS, Bodnar RJ, Law RD (2015) Significance of "stretched" mineral inclusions for reconstructing P–T exhumation history. Contrib Mineral Petrol. https://doi.org/10.1007/s00410-015-1149-0
- Ashley KT, Steele-MacInnis M, Bodnar RJ, Darling RS (2016) Quartz-in-garnet inclusion barometry under fire: reducing uncertainty from model estimates. Geology 44:699–702. https://doi.org/10.1130/G38211.1
- Avadanii D (2017) A new barometer from stress fields around inclusions. PhD thesis, University of Oxford
- Bose K, Ganguly J (1995) Quartz-coesite transition revisited; reversed experimental determination at 500–1200 degrees C and retrieved thermochemical properties. Am Mineral 80:231–238. https://doi. org/10.2138/am-1995-3-404
- Boyd FR, England JL (1960) The quartz-coesite transition. J Geophys Res 65:749–756. https://doi.org/10.1029/JZ065i002p00749
- Castro AE, Spear FS (2016) Reaction overstepping and re-evaluation of peak P–T conditions of the blueschist unit Sifnos, Greece: implications for the cyclades subduction zone. Int Geol Rev. https://doi.org/10.1080/00206814.2016.1200499
- Dean KJ, Sherman WF, Wilkinson GR (1982) Temperature and pressure dependence of the Raman active modes of vibration of α-quartz. Spectrochim Acta Part Mol Spectrosc 38:1105–1108. https://doi.org/10.1016/0584-8539(82)80044-5
- Enami M, Nishiyama T, Mouri T (2007) Laser Raman microspectrometry of metamorphic quartz: a simple method for comparison of metamorphic pressures. Am Mineral 92:1303–1315. https://doi.org/10.2138/am.2007.2438
- Guiraud M, Powell R (2006) P–V–T relationships and mineral equilibria in inclusions in minerals. Earth Planet Sci Lett 244:683–694. https://doi.org/10.1016/j.epsl.2006.02.021
- Hemley RJ (1987) Pressure dependence of Raman spectra of SiO₂ polymorphs: α-quartz, coesite, and stishovite. In: Manghnani MH, Syono Y (eds) Geophysical monograph series. American Geophysical Union, Washington, DC, pp 347–359
- Holland TJB (1980) The reaction albite=jadeite+quartz determined experimentally in the range 600–1200 °C. Am Mineral 65:129–134
- Holland TJB, Powell R (2004) An internally consistent thermodynamic data set for phases of petrological interest: an internally consistent thermodynamic dataset. J Metamorph Geol 16:309–343. https://doi.org/10.1111/j.1525-1314.1998.00140.x
- Holland TJB, Powell R (2011) An improved and extended internally consistent thermodynamic dataset for phases of petrological interest, involving a new equation of state for solids: thermodynamic dataset for phases of petrological interest. J Metamorph Geol 29:333–383. https://doi.org/10.1111/j.1525-1314.2010.00923.x
- Howell D, Wood IG, Dobson DP et al (2010) Quantifying strain birefringence halos around inclusions in diamond. Contrib Mineral Petrol 160:705–717. https://doi.org/10.1007/s00410-010-0503-5
- Jakobsson S (2012) Oxygen fugacity control in piston-cylinder experiments. Contrib Mineral Petrol 164:397–406. https://doi. org/10.1007/s00410-012-0743-7
- Kitahara S, Kennedy GC (1964) The quartz–coesite transition. J Geophys Res 69:5395–5400. https://doi.org/10.1029/JZ069i024p 05395
- Kohn MJ (2014) "Thermoba-Raman-try": calibration of spectroscopic barometers and thermometers for mineral inclusions. Earth Planet Sci Lett 388:187–196. https://doi.org/10.1016/j.epsl.2013.11.054
- Kohn M, Spear FS (1991a) Error propagation for barometers: 2. Application to rocks. Am Mineral 76:138–147

- Kohn M, Spear FS (1991b) Error propagation for barometers: 1. Accuracy and precision of experimentally located end-member reactions. Am Mineral 76:128–137
- Korsakov AV, Perraki M, Zhukov VP et al (2009) Is quartz a potential indicator of ultrahigh-pressure metamorphism? Laser Raman spectroscopy of quartz inclusions in ultrahigh-pressure garnets. Eur J Mineral 21:1313–1323. https://doi.org/10.1127/0935-1221/2009/0021-2006
- Kouketsu Y, Nishiyama T, Ikeda T, Enami M (2014) Evaluation of residual pressure in an inclusion-host system using negative frequency shift of quartz Raman spectra. Am Mineral 99:433–442. https://doi.org/10.2138/am.2014.4427
- Liu L, Mernagh TP (1992) High-pressure Raman study of the a-quartz forms of SiO_2 and GeO_2 at room temperature. High Temp-High Press 24:13-21
- Mazzucchelli ML, Burnley P, Angel RJ et al (2018) Elastic geothermobarometry: corrections for the geometry of the host-inclusion system. Geology 46:231–234. https://doi.org/10.1130/G39807.1
- McDade P, Wood BJ, Van Westrenen W et al (2002) Pressure corrections for a selection of piston-cylinder cell assemblies. Mineral Mag 66:1021–1028. https://doi.org/10.1180/0026461026660074
- Milani S, Nestola F, Alvaro M et al (2015) Diamond–garnet geobarometry: the role of garnet compressibility and expansivity. Lithos 227:140–147. https://doi.org/10.1016/j.lithos.2015.03.017
- Mirwald PW, Massonne H-J (1980) The low-high quartz and quartz-coesite transition to 40 kbar between 600 and 1600 °C and some reconnaissance data on the effect of NaAlO₂ component on the low quartz-coesite transition. J Geophys Res 85:6983. https://doi.org/10.1029/JB085iB12p06983
- Mirwald PW, Getting IC, Kennedy GC (1975) Low-friction cell for piston-cylinder high-pressure apparatus. J Geophys Res 80:1519–1525. https://doi.org/10.1029/JB080i011p01519
- Powell R, Holland TJB (2008) On thermobarometry. J Metamorph Geol 26:155–179. https://doi.org/10.1111/j.1525-1314.2007.00756.x
- Rosenfeld JL (1969) Stress effects around quartz inclusions in almandine and the piezothermometry of coexisting aluminum silicates. Am J Sci 267:317–351. https://doi.org/10.2475/ajs.267.3.317
- Rosenfeld JL, Chase AB (1961) Pressure and temperature of crystallization from elastic effects around solid inclusions in minerals? Am J Sci 259:519–541. https://doi.org/10.2475/ajs.259.7.519
- Schmidt C, Ziemann MA (2000) In-situ Raman spectroscopy of quartz: a pressure sensor for hydrothermal diamond-anvil cell experiments at elevated temperatures. Am Mineral 85:1725–1734. https://doi.org/10.2138/am-2000-11-1216
- Sorby HC, Butler PJ (1868) On the structure of rubies, sapphires, diamonds, and some other minerals. Proc R Soc Lond 17:291–302. https://doi.org/10.1098/rspl.1868.0050
- Spear FS, Thomas JB, Hallett BW (2014) Overstepping the garnet isograd: a comparison of QuiG barometry and thermodynamic modeling. Contrib Mineral Petrol. https://doi.org/10.1007/s00410-014-1059-6
- Trail D, Bruce Watson E, Tailby ND (2012) Ce and Eu anomalies in zircon as proxies for the oxidation state of magmas. Geochim Cosmochim Acta 97:70–87. https://doi.org/10.1016/j.gca.2012.08.032
- Van der Molen I, Van Roermund HLM (1986) The pressure path of solid inclusions in minerals: the retention of coesite inclusions during uplift. Lithos 19:317–324. https://doi.org/10.1016/0024-4937(86)90030-7
- Wang Z, Ji S (2001) Elasticity of six polycrystalline silicate garnets at pressure up to 3.0 GPa. Am Mineral 86:1209–1218. https://doi.org/10.2138/am-2001-1009
- Worley P (2000) High-precision relative thermobarometry: theory and a worked example. J Metamorph Geol 18:91–101. https://doi.org/10.1046/j.1525-1314.2000.00239.x



42

- Yagii T, Akaogi M, Shimomurad O et al (1987) High pressure and high temperature equations of state of majorite. In: Manghnani MH, Syono Y (eds) Geophysical monograph series. American Geophysical Union, Washington, DC, pp 141–147
- Zhang Y (1998) Mechanical and phase equilibria in inclusion—host systems. Earth Planet Sci Lett 157:209–222. https://doi.org/10.1016/S0012-821X(98)00036-3
- Zhang M, Scott J (2007) Raman studies of oxide minerals: a retrospective on cristobalite phases. J Phys Condens Matter 19:275201
- Zhang L, Ahsbahs H, Kutoglu A, Geiger CA (1999) Single-crystal hydrostatic compression of synthetic pyrope, almandine, spessartine, grossular and andradite garnets at high pressures. Phys Chem Miner 27:52–58. https://doi.org/10.1007/s002690050240
- Zhukov VP, Korsakov AV (2015) Evolution of host-inclusion systems: a visco-elastic model. J Metamorph Geol 33:815–828. https://doi.org/10.1111/jmg.12149

